Control Methods of Inverter-Interfaced Distributed Generators in a Microgrid System

Il-Yop Chung, *Member, IEEE*, Wenxin Liu, *Member, IEEE*, David A. Cartes, *Senior Member, IEEE*, Emmanuel G. Collins, Jr. *Senior Member, IEEE* and Seung-Il Moon, *Member, IEEE*

***Abstract* – Microgrids are a new concept for future energy distribution systems that enable renewable energy integration and improved energy management capability. Microgrids consist of multiple distributed generators (DGs) that are usually integrated via power-electronic inverters. In order to enhance power quality and power distribution reliability, microgrids need to operate in both grid-connected and island modes. Consequently, microgrids can suffer performance degradation as the operating conditions vary due to abrupt mode changes and variations in bus voltages and system frequency. This paper presents controller design and optimization methods to stably coordinate multiple inverter-interfaced distributed generators and to robustly control individual interface-inverters against voltage and frequency disturbances. Droop control concepts are used as system-level multiple DG coordination controllers and L_1 control theory is applied to device-level inverter controllers. Optimal control parameters are obtained by Particle Swarm Optimization algorithms and the control performance is verified via simulation studies.**

***Index Terms* – Microgrid, distributed generator (DG), droop controller, optimal control, L_1 theory, particle swarm optimization (PSO), control parameter tuning**

I. Introduction

RECENTLY, due to the development of power electronics and information technology, the performance and efficiency of distributed generators (DGs) has been significantly improved. Inverter-interfaced DGs can be flexibly deployed in power systems in order to mitigate peak loads and improve power quality and reliability. Microgrids constitute an advanced concept for application of DGs and enable integration of multiple DGs and autonomous islanding operation according to power system conditions [1-6]. Microgrids are designed as autonomous cells in power systems, which might include sensitive loads and multiple distributed generators (DGs) [1]. These features can bring lots of flexibility to power distribution control but also pose complex control problems.

Normally, microgrids operate in parallel to the grids because the grids can support the system frequency and bus voltages by covering the power mismatch immediately. When a fault occurs someplace in the grids, microgrids need to operate independently from the grid to supply uninterrupted power to the loads. The control method presented in this paper is to improve the controlled performance of microgrids by coordinating the output powers of multiple DGs in microgrids for the two considerations of operation (i.e., integration of multiple DGs and autonomous island operation) and by optimizing the control parameters. To this end, this paper applies droop controllers that can automatically assign the amount of power sharing for load changes without communication [7-10].

In the island mode, the bus voltages and the system frequency may vary with certain amount of uncertainties because the droop controllers adjust them to cover up instant power mismatch. This paper also focuses on controller design for individual power inverters that accommodates variations in the bus voltages and the system frequency. Many design theories have been developed for optimal disturbance rejection, most notably, H_2 and H_∞ control [11-16]. H_2 control considers white noise disturbances and H_∞ control considers energy-bounded L_2 disturbances [11]. In contrast, L_1 theory considers persistent bounded uncertain disturbances (L_∞ disturbances) [13-16]. Since the disturbances in the voltage and system frequency are persistent due to continual power mismatch in microgrids, especially during island mode, L_1 theory is the most relevant in capturing the features of the disturbances and is used in this research.

This paper proposes novel controller optimization algorithms for the droop controllers and inverter output controllers for inverter-interfaced DGs using Particle Swarm Optimization (PSO). Since the PSO is a derivative-free and population-based stochastic search algorithm, it has outstanding ability to escape local minima and less sensitivity to the complexity of the system [17]. PSO algorithms are used in the inverter output controllers associated with L_1 theory and the droop controllers with a time-weighted error-integrating cost function. Control performance, power quality, and robustness are considered during controller optimization processes.

This work was supported in part by Florida Energy Systems Consortium (FESC) and the Institute for Energy Systems, Economics and Sustainability (IESES) at Florida State University, Tallahassee, FL, USA.

I. Chung, D.A. Cartes and E.G. Collins, Jr. are with Florida State University, Tallahassee, FL, USA (e-mail: chung@caps.fsu.edu, dave@caps.fsu.edu, ecollins@eng.fsu.edu).

W. Liu is with the Klipsch School of Electrical and Computer Engineering at New Mexico State University, Las Cruces, NM, USA (e-mail: wliu@nmsu.edu)

S. Moon is with the School of Electrical Engineering and Computer Science at Seoul National University, Seoul, South Korea (e-mail: moonsi@plaza.snu.ac.kr).

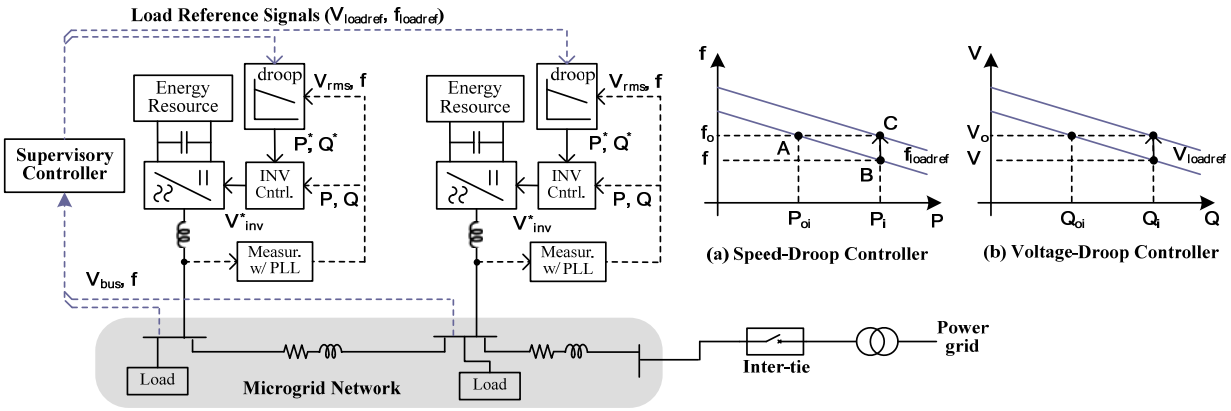

Fig. 1 Concept of multiple DG coordination control using droop controllers in a microgrid

II. Microgrid Control

A. Problem Statement

This paper focuses on how to design microgrid controllers and to determine the control parameters for the droop controllers (system-level) and inverter output controllers (device-level). The most critical problem for control parameter optimization is the complexity of overall systems due to the high state dimensions and nonlinearity of microgrids. Common approaches are based on small-signal linearization but small-signal models intrinsically depend on specific operating points.

In our previous research [17], Particle Swarm Optimization (PSO) algorithm was applied directly to a power-electronic-switch-level microgrid simulation model instead of small-signal models. Optimization was performed at various operating conditions to accommodate the system nonlinearity and yielded good performance. However, since the control parameters were optimized all together regardless of levels or types of controllers, it is hard to analyze the effects of individual control parameters on overall performances. In this paper, we propose to modularize controller design processes and optimize parameters step-by-step to evaluate the optimization performance.

Reference [4] showed that there are three control modes in microgrid control: high, medium, and low frequency modes. According to sensitivity analysis [10], the sensitivity of a certain parameter to a specific mode, defined in the Appendix, is especially large whereas the sensitivities to other modes are negligible. For example, the high-frequency modes are correlated to the DG output circuits such as inverter output filters. Medium frequency modes are associated with the inverter output voltage and current controllers. The droop controllers are linked to low-frequency modes so that they have a significant effect on system stability [18]. This fact supports our objective to independently tune the parameters of each controller. Therefore, this paper proposes two controller optimization methods for microgrid DG controllers: the first optimization objective is to make the individual inverter output controller robust with respect to changes in the operating conditions. Second, the droop control parameter optimization is to enhance system-wide stable operation.

B. Microgrid System Model and Control Concept

Fig. 1 presents a schematic of a microgrid that includes multiple inverter-interfaced DGs. The microgrid is connected to the grid through an inter-tie breaker. During normal operation, the microgrid becomes a part of a distribution system. Then, the grid can maintain the voltage of the point of common coupling and the system frequency. When a fault occurs in the grid, the microgrid operates in the island mode by disconnecting the inter-tie breaker, thereby increasing the reliability of the microgrid [19]. In the island mode, DGs are required to share the power mismatch instantly in order to follow load demands and also to maintain power quality.

As shown in Fig. 1, the DG controllers are composed of two controllers: DG coordination controllers and inverter output controllers. The coordination controllers need to calculate the output power references whereas the inverter controllers should control the inverter output voltages.

According to previous studies [3-9], droop controllers have turned out the most effective method to coordinate power generation between multiple DGs because they can immediately adjust power outputs to stabilize the system and also do not need instant communication between units. The speed- and voltage-droop controllers are applied for real and reactive power sharing as shown in Fig. 1(a) and Fig. 1(b). The droop controllers can be expressed as

$$P_i^* = P_{oi} + (f_o + f_{loadref} - f)/R_i \quad (1)$$

$$Q_i^* = Q_{oi} + (V_{oi} + V_{loadref} - V_i)/M_i \quad (2)$$

where i is the DG index; R_i and M_i are droop parameters; P_i, Q_i, V_i, and f are locally measured real and reactive power, bus root-mean-square voltage, and the system frequency, respectively; the subscript o represents the preset values of normal operating points. In most cases, f_o and V_o are the nominal values. Different settings of the droop constants can assign different amounts of power sharing between DGs.

Since the droop controller changes system frequency or bus voltages to damp the power mismatches, the bus voltage and frequency variation can occur especially in the island mode. To maintain the voltages and frequency close to the nominal values, the load reference signals are periodically sent by the

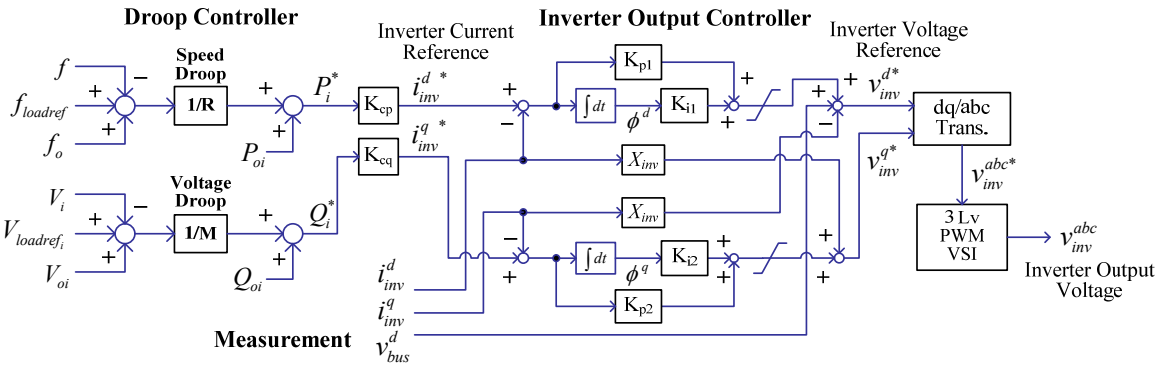

Fig. 2 Control block diagram for inverter-interfaced DGs (all variables are represented in per unit)

microgrid management system with certain time delay. $f_{loadref}$ and $V_{loadref}$ are the load reference signals of frequency and voltage, respectively.

The droop controller of inverters imitates the control of synchronous generators. Therefore, the mechanism of load frequency control of the microgrid is the same as the power grid. The PLL circuits of power inverters can eliminate fast frequency deviation in the DG output power by employing relevant low pass filters. The system frequency can be maintained in case the power mismatch can be recovered immediately. Hence, enough power reserve or energy storage is required to maintain system stability. In this paper, it is assumed that the DGs are designed to have enough power ratings to cover load variation in the microgrid.

Fig. 2 shows the control block diagram of inverter-interfaced DGs in the d-q rotating reference frame. Since the d-q transformation decouples real and reactive powers, the d- and q-axis inverter output current references can be obtained from real and reactive power references, respectively. Details of the d-q transformation and its sign convention are explained in the Appendix.

The droop controllers generate the real and reactive power references according to the droop characteristics of (1) and (2). The inverter output controllers generate the inverter voltage references with PI controllers. In this paper, three-level PWM inverters, which contain less harmonic components, are used. The equations of the inverter output controller are

$$\frac{d}{dt}\phi^d = i_{inv}^{d\,*} - i_{inv}^d \tag{3}$$

$$\frac{d}{dt}\phi^q = i_{inv}^{q\,*} - i_{inv}^q \tag{4}$$

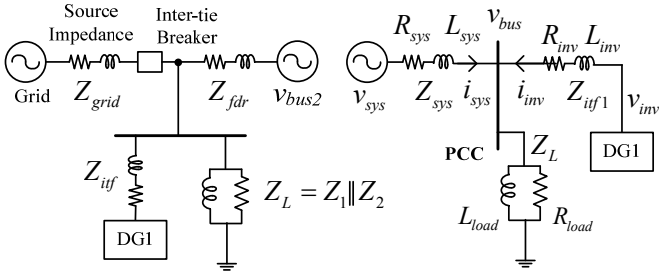

(a) Microgrid simplified circuit model (b) Microgrid equivalent model

Fig. 3 Microgrid equivalent circuit model

$$v_{inv}^{d\,*} = K_{p1}\cdot\left(i_{inv}^{d\,*} - i_{inv}^d\right) + K_{i1}\cdot\phi^d - X_{inv}\cdot i_{inv}^q + v_{bus}^d \tag{5}$$

$$v_{inv}^{q\,*} = K_{p2}\cdot\left(i_{inv}^{q\,*} - i_{inv}^q\right) + K_{i2}\cdot\phi^q + X_{inv}\cdot i_{inv}^d \tag{6}$$

C. Mathematical Model for Inverter Controller Tuning

The inverter output controller is a device-level controller whose performance is affected by the inverter output circuits and the bus voltages and system frequency. The bus voltage characteristics depend on the interaction between the corresponding DG and the rest of the system. The optimization objective is to make the inverter output controller robust with respect to disturbances such as variations in bus voltages and frequency.

The microgrid system shown in Fig. 1 can be simplified from the perspective of DG1 as shown in Fig. 3. The mathematical equation of the microgrid power circuit can be obtained from Fig. 3 (b) as

$$\frac{d}{dt}i_{inv}^d = -\frac{R_{inv}}{L_{inv}}i_{inv}^d + w_S\cdot i_{inv}^q + \frac{1}{L_{inv}}\left(v_{inv}^d - v_{bus}^d\right) \tag{7}$$

$$\frac{d}{dt}i_{inv}^q = -\frac{R_{inv}}{L_{inv}}i_{inv}^q - w_S\cdot i_{inv}^d + \frac{1}{L_{inv}}\left(v_{inv}^q - v_{bus}^q\right) \tag{8}$$

$$\frac{d}{dt}i_{sys}^d = -\frac{R_{sys}}{L_{sys}}i_{sys}^d + w_S\cdot i_{sys}^q + \frac{1}{L_{sys}}\left(v_{sys}^d - v_{bus}^d\right) \tag{9}$$

$$\frac{d}{dt}i_{sys}^q = -\frac{R_{sys}}{L_{sys}}i_{sys}^q - w_S\cdot i_{sys}^d + \frac{1}{L_{sys}}\left(v_{sys}^q - v_{bus}^q\right) \tag{10}$$

$$\frac{d}{dt}i_L^d = \frac{1}{L_{load}}v_{bus}^d + w_S\cdot i_L^q \tag{11}$$

$$\frac{d}{dt}i_L^q = \frac{1}{L_{load}}v_{bus}^q - w_S\cdot i_L^d \tag{12}$$

$$v_{bus}^d = R_{load}\cdot i_{inv}^d + R_{load}\cdot i_{sys}^d - R_{load}\cdot i_L^d \tag{13}$$

$$v_{bus}^q = R_{load}\cdot i_{inv}^q + R_{load}\cdot i_{sys}^q - R_{load}\cdot i_L^q \tag{14}$$

Since the PWM inverter circuit and output filter have faster characteristics than the inverter output controller, it is reasonable to assume that the inverter actual output voltage can follow the inverter voltage references fast enough. Then, the small-signal closed-loop model can be obtained as Fig. 4 where x, x_c, u, w, m, and y represent the vectors of the plant

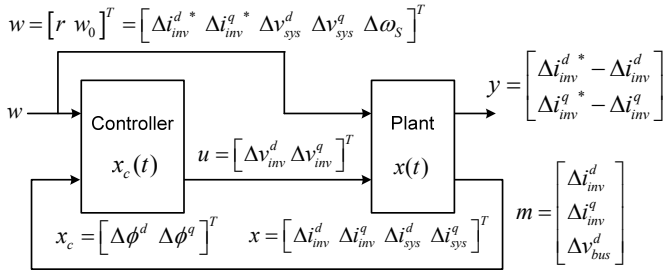

Fig. 4 Closed loop control block diagram

states, controller states, control inputs, disturbance inputs, measured outputs, and performance variables, respectively. The small-signal state-space equations of microgrid circuits can be obtained from (7) through (14) as

$$\dot{x}(t)=Ax(t)+\begin{bmatrix}B_u & B_w\end{bmatrix}\begin{bmatrix}u(t)\\ w(t)\end{bmatrix} \tag{15}$$

$$\begin{bmatrix}m(t)\\ y(t)\end{bmatrix}=\begin{bmatrix}C_m\\ C_y\end{bmatrix}x(t)+\begin{bmatrix}0 & D_{mw}\\ D_{yu} & D_{yw}\end{bmatrix}\begin{bmatrix}u(t)\\ w(t)\end{bmatrix} \tag{16}$$

The small-signal state-space model of the controller also can be obtained from (3) through (6) as

$$\dot{x}_c(t)=A_cx_c(t)+\begin{bmatrix}B_{cw} & B_{cm}\end{bmatrix}\begin{bmatrix}w(t)\\ m(t)\end{bmatrix} \tag{17}$$

$$u(t)=C_cx_c(t)+\begin{bmatrix}D_{cw} & D_{cm}\end{bmatrix}\begin{bmatrix}w(t)\\ m(t)\end{bmatrix} \tag{18}$$

Then, the closed-loop small-signal state-space model can be derived from (15) through (18) as

$$\dot{\tilde{x}}(t)=A_{cl}\tilde{x}(t)+B_{cl}w(t),\quad \tilde{x}(0)=0 \tag{19}$$

$$y(t)=C_{cl}\tilde{x}(t)+D_{cl}w(t) \tag{20}$$

where $\tilde{x}(t)=\left[x(t)\ x_c(t)\right]^T$ denotes the closed-loop state and

$$A_{cl}=\begin{bmatrix}A+B_uD_{cm}C_m & B_uC_c\\ B_{cm}C_m & A_c\end{bmatrix},\ B_{cl}=\begin{bmatrix}B_w+B_uD_{cw}\\ B_{cw}\end{bmatrix},$$

$$C_{cl}=\begin{bmatrix}C_y+D_{yu}D_{cm}C_m & D_{yu}C_c\end{bmatrix},\ D_{cl}=D_{yu}D_{cw}+D_{yw}.$$

Fig. 5 illustrates the closed-loop pole loci when the inverter output control parameters change. According to the participation factors, it is found that Mode 3 and 4 are sensitive to the

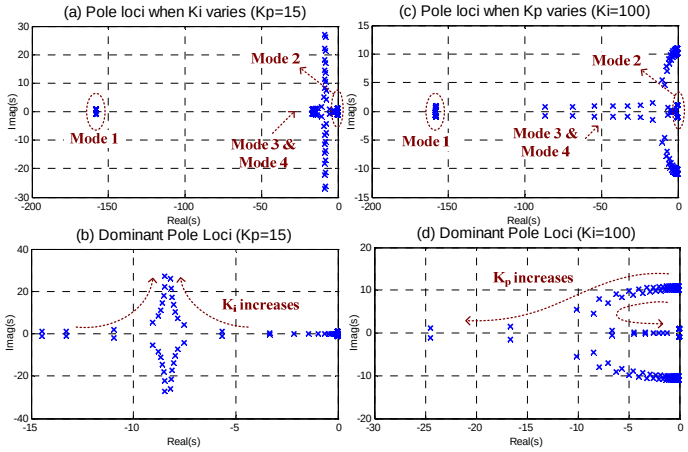

Fig. 5 Closed-loop eigenvalue analysis

inverter control parameter changes, whereas Modes 1 and 2 are tightly related to the power system parameters such as system resistance and inductance. Therefore, to achieve high control performance, the location of the eigenvalues of Mode 3 and 4 should be carefully located. Detailed controller design procedure will be presented in the next section.

III. Optimization Algorithm

A. Particle Swarm Optimization (PSO)

PSO is a population-based intelligent searching algorithm. It has excellent performance for searching the global optimum because it can diversify the swarm with a stochastic velocity term. PSO resembles the social behavior of birds or bees when they find food together in a field [21-23]. The performance of this evolutionary algorithm is based on the intelligent movement of each particle and collaboration of the swarm. In the standard version of PSO, each particle starts from a random location and searches the space with its own best knowledge and the swarm's best experience. The search rule can be expressed by simple equations with respect to the position vector $X_i=[x_{i1},\ldots,x_{in}]$ and the velocity vector $V_i=[v_{i1},\ldots,v_{in}]$ in the n-dimensional search space as

$$V_i^{k+1}=wV_i^k+c_1\cdot rd_1(X_{pb_i}^k-X_i^k)+c_2\cdot rd_2(X_{gb}^k-X_i^k) \tag{21}$$

$$X_i^{k+1}=X_i^k+V_i^{k+1} \tag{22}$$

$$A_{cl}=\begin{bmatrix}
-\frac{R_{inv}+K_{p1}}{L_{inv}} & W_S-\frac{X_{inv}}{L_{inv}} & 0 & 0 & 0 & 0 & \frac{K_{i1}}{L_{inv}} & 0\\
-W_S+\frac{X_{inv}}{L_{inv}} & -\frac{R_{inv}+R_{load}+K_{p2}}{L_{inv}} & 0 & -\frac{R_{load}}{L_{inv}} & 0 & \frac{R_{load}}{L_{inv}} & 0 & \frac{K_{i2}}{L_{inv}}\\
-\frac{R_{load}}{L_{sys}} & 0 & -\frac{R_{sys}+R_{load}}{L_{sys}} & W_S & \frac{R_{load}}{L_{sys}} & 0 & 0 & 0\\
0 & -\frac{R_{load}}{L_{sys}} & -W_S & -\frac{R_{sys}+R_{load}}{L_{sys}} & 0 & \frac{R_{load}}{L_{sys}} & 0 & 0\\
\frac{R_{load}}{L_{load}} & 0 & \frac{R_{load}}{L_{load}} & 0 & -\frac{R_{load}}{L_{load}} & W_S & 0 & 0\\
0 & \frac{R_{load}}{L_{load}} & 0 & \frac{R_{load}}{L_{load}} & -W_S & -\frac{R_{load}}{L_{load}} & 0 & 0\\
-1 & 0 & 0 & 0 & 0 & 0 & 0 & 0\\
0 & -1 & 0 & 0 & 0 & 0 & 0 & 0
\end{bmatrix},\ B_{cl}=\begin{bmatrix}
\frac{K_{p1}}{L_{inv}} & 0 & 0 & 0 & I_{inv}^q\\
0 & \frac{K_{p2}}{L_{inv}} & 0 & 0 & -I_{inv}^d\\
0 & 0 & \frac{1}{L_{sys}} & 0 & I_{sys}^q\\
0 & 0 & 0 & \frac{1}{L_{sys}} & -I_{sys}^d\\
0 & 0 & 0 & 0 & I_L^q\\
0 & 0 & 0 & 0 & -I_L^d\\
1 & 0 & 0 & 0 & 0\\
0 & 1 & 0 & 0 & 0
\end{bmatrix},$$

$$C_{cl}=\begin{bmatrix}-1 & 0 & 0 & 0 & 0 & 0 & 0 & 0\\ 0 & -1 & 0 & 0 & 0 & 0 & 0 & 0\end{bmatrix},\quad D_{cl}=\begin{bmatrix}1 & 0 & 0 & 0 & 0\\ 0 & 1 & 0 & 0 & 0\end{bmatrix}$$

$$w = w_{max} - \frac{k \cdot (w_{max} - w_{min})}{N} \tag{23}$$

where, i, k and N are the particle, the iteration index and the number of total iterations, respectively; V_i^k and X_i^k are the velocity and position vectors of particle i at iteration k, respectively; w is the inertia weight; c_1 and c_2 are two positive constants normally set to 2.0; rd_1 and rd_2 are random numbers in [0,1]; X_{pbi}^k and X_{gb}^k are the best positions that particle i has achieved so far based on its own experience and the swarm's best experience, respectively.

Boundaries of search space represent certain physical limitations and restrictions on the parameters. According to previous research, it is difficult to find optimal solutions located near the boundaries. To solve this problem, the damped reflecting boundary method [22], which is more robust and consistent in finding a solution near the boundaries, is used in this paper. The idea is that when the j_{th} element of the i_{th} particle (x_{ij}^{k+1}) crosses the boundary (x_j^{lim}), the position vector and velocity vector are changed to

$$\begin{aligned} X_i^{k+1} &= \left[\cdots, x_{i(j-1)}^k, \; x_j^{lim}, \; x_{i(j+1)}^k, \; \cdots \right] \\ V_i^{k+1} &= \left[\cdots, v_{i(j-1)}^k, \; -rd \cdot v_{ij}^k, \; v_{i(j+1)}^k, \cdots \right] \end{aligned} \tag{24}$$

where, rd is a random number in [0,1].

B. Inverter Output Controller Optimization

This paper applies L_1 theory to design robust inverter output controllers. The L_1 theory is more appropriate in situations involving persistent, unknown but bounded exogenous disturbances compared to other robust control theories such as H_2 and H_∞ theories. Using the L_1 theory, the inverter output controller can be designed to have effective disturbance rejection in the presence of voltage and frequency variations in the microgrids.

The inverter output controller design criteria are as follows:

i) The undisturbed closed-loop system (19) and (20) should be asymptotically stable. (Stability criterion)
ii) The inverter control bandwidth should be large enough to follow fast changes in output power references. (Controller criterion)
iii) The L_∞ norm of the performance variable $y(t)$ in (20) should be minimized against persistent, bounded disturbances $w(t)$. (Performance criterion)

The first criterion means the closed-loop system matrix A_{cl} must be Hurwitz, which means all the closed-loop poles are located in the LHP. The second criterion is related to the location of the eigenvalues of the closed-loop system in s-plane. The third criterion can be achieved by minimizing L_1 norm of the convolution operator as

$$\|G\|_1 = \sup_{w(\cdot) \in L_\infty} \frac{\|y\|_{\infty,\infty}}{\|w\|_{\infty,2}} \tag{25}$$

where the definitions of two ∞-norms are explained in the Appendix. The L_1 norm of (25) can capture the worst-case peak amplitude response of $y(t)$, which represents control errors as shown in Fig. 4, due to persistent disturbances $w(t)$ in bus voltages and the system frequency.

If the first criterion is satisfied, $\|G\|_1$ is bounded, which means the closed-loop system (19) and (20) is bounded input bounded output stable. Therefore, the meaning of the minimization of (25) can be equivalent to minimizing the effects of the voltage and frequency disturbances to the current control performance of the inverter.

The L_1 optimal control problem was formulated by M. Vidyasagar but the optimal L_1 controllers are irrational and hence impractical [13-14]. To resolve the problem, this paper applies a new method to minimize an upper bound on the L_1 norm, which is proposed by V. Chellaboina *et al* [15].

Assume that there exists a positive-definite matrix Q satisfying an algebraic Lyapunov equation such as

$$0 = A_{cl}Q + QA_{cl}^T + \alpha Q + \frac{1}{\alpha} B_{cl} B_{cl}^T \tag{26}$$

where $\alpha > 0$. Then, A_{cl} is Hurwitz and the L_1 norm of the convolution operator G satisfies the bound

$$\|G\|_1^2 \le \sigma_{max}\left(C_{cl} Q C_{cl}^T\right) + \sigma_{max}\left(D_{cl} D_{cl}^T\right) \tag{27}$$

The proof of (27) can be found in [15] and is summarized in the Appendix. Since the algebraic Lyapunov equation of (26) has a positive-definite solution of Q if and only if $A_{cl}+(\alpha/2)I_n$ is Hurwitz where I_n is an identity matrix, the positive number α should satisfy

$$0 < \alpha < -2\alpha_R(A_{cl}) \tag{28}$$

where $\alpha_R(A_{cl})$ denotes the spectral abscissa of A_{cl}. Then, the tightest upper bound for the L_1 norm of the convolution operator G can be obtained as

$$\|G\|_1^2 \le \inf_{0 < \alpha < -2\alpha_R(A_{cl})} \left\{ \sigma_{max}\left(C_{cl} Q C_{cl}^T\right) + \sigma_{max}\left(D_{cl} D_{cl}^T\right) \right\} \tag{29}$$

The control parameters (K_p and K_i) and the positive number α should be chosen to optimize the right hand side of (29), which defines an upper bound on the L_1 norm. Some references proposed a gradient-based optimization which requires a differentiable cost function [14-15]. Since the right hand side of (29) is not differentiable, reference [15] tried to find another upper bound of the upper bound of L_1 norm using matrix trace functions. However, the problems of their methods are that the solving process is complex and the methods result in a more conservative upper bound of $\|G\|_1$.

To optimize the upper bound inherent in (29) this paper proposes a new double-layer PSO algorithm. Since the PSO algorithm is based on population-based intelligent optimization, we do not need to use a trace function for optimization. To meet the three design criteria for inverter output controller, the penalty function and cost functions are proposed as

$$J = \sum_{i=1}^{3} f_i \tag{30}$$

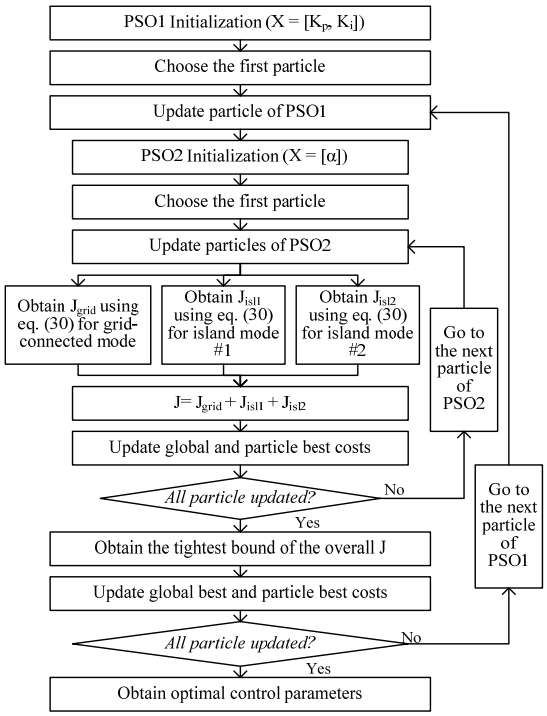

Fig. 6 Parameter tuning process using double-layer PSO

where

$$f_1 = \begin{cases} 0, & \text{if } A_{cl} \text{ is Hurwitz} \\ 10,000, & \text{otherwise} \end{cases} \tag{31}$$

$$f_2 = \left| Real(\lambda_C) \right|^{-1} \tag{32}$$

$$f_3 = \inf_{0<a<-2a_R(A_{cl})} \left\{ \sigma_{max}\left(C_{cl} Q C_{cl}^{\ T}\right) + \sigma_{max}\left(D_{cl} D_{cl}^{\ T}\right) \right\}^{1/2} \tag{33}$$

and λ_C is the dominant eigenvalue of Mode 3 and 4 of the closed-loop system. The penalty function f_1 penalizes for unstable cases. The cost function f_2 is for enough controller bandwidth. The cost function f_3 is for controller robustness by obtaining the tightest bound of the L_1 norm of G.

Fig. 6 shows the overall optimization process of the double-layer PSO algorithm. Note that there are two optimization loops using PSO algorithms. The outer PSO loop (PSO1) is to find the control parameters such as [K_p, K_i] whereas the inner PSO loop (PSO2) is to find the tightest bound of the cost function depending on [α] for the set of K_p and K_i given by PSO1. The cost function (30) is evaluated in three operating conditions.

C. Droop Controller Optimization

Whereas the design criteria of the inverter output controller are stability and robustness of each individual inverter, the criteria of droop control optimization are the system-wide stability and power quality. Specifically, the following criteria need to be satisfied:

i) The overall microgrid should stably and efficiently control DG output power according to the power reference or load demands.

ii) The voltages and frequency of the microgrid should be securely maintained near nominal values (13.8kV and 60Hz).

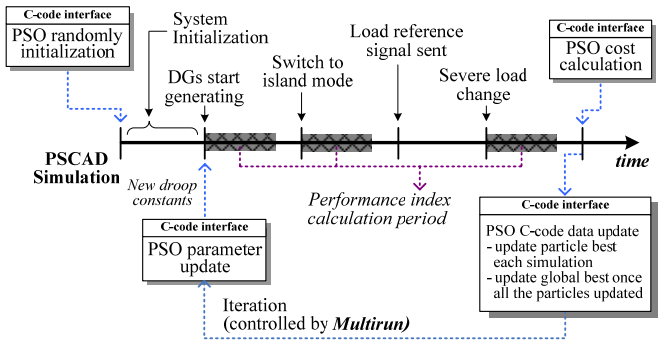

Fig. 7 Droop controller optimization using PSCAD/EMTDC Multirun simulation sequences

The linearization of the complete microgrid system for droop controller optimization may result in severe discrepancies with the actual nonlinear microgrid system. Therefore, in this paper, a power-electronic-switch-level simulation model using PSCAD/EMTDC, which is a professional electromagnetic transient power system simulation tool, is used for optimization instead of a small-signal model.

The controller optimization can be done by minimizing an error-integrating cost function, which can yield a stable system with small steady-state errors. There are four types of error-minimizing cost functions such as IAE (integrated absolute error), ISE (integrated squared error), ITAE (integrated time-weighted absolute error), and ITSE (integrated time-weighted squared error). According to a previous study [24], the ITAE yields the best performance for the objectives.

To satisfy the first criterion under various operation conditions, three conditions are considered: 1) the grid-connected mode (J_1), 2) the transition period between the grid-connected and the island mode (J_2), and 3) the island mode (J_3). Then the cost function can be designed as

$$J = \sum_{i=1}^{3} J_i = \sum_{i=1}^{3} \left[\sum_{k=K_o^i}^{K_f^i} (k - K_o^i) \cdot W \cdot \left| E^i(k) \right| \right] \tag{34}$$

where, i and k are the control performance index and the sampled simulation time, respectively; K_o^i and K_o^f are the starting and ending time for calculating each control performance index; W is a weighting matrix, $E^i(k)$ is the absolute error matrix defined as

$$E^i(k) = \left[\Delta P^i(k),\ \Delta Q^i(k),\ \Delta V^i(k),\ \Delta freq^i(k) \right]^{\mathrm{T}} \tag{35}$$

The first and second element, $\Delta P(k)$ and $\Delta Q(k)$, represent the error between the real and reactive power references and measurements. The third and fourth elements, $\Delta V(k)$ and $\Delta freq(k)$, mean the voltage and frequency deviation from the nominal values (1.0 *p.u.*). The weighting matrix is set to [1.0, 1.0, 0.5, 0.5]. The particles are composed of the droop coefficients such as [R_o, M_o]. Then, the actual droop control parameters can be obtained as

$$R_i = R_o \cdot r_i,\ M_i = M_o \cdot m_i \quad (36)$$

where r_i and m_i are constants. In this paper, r_i are arbitrarily set to 0.05, and 0.07; all m_i are set to 0.05. These values mean the inverse of the power sharing ratio between DGs such as 1/5: 1/7 for real power and 1:1 for reactive power.

Fig. 7 illustrates the droop controller optimization process through the PSCAD/EMTDC *multirun* function. Each simulation contains three control performance evaluations as explained in (34). For facilitating simulation speed, the data during the initialization period (between 0.0 to 0.2 seconds) are stored to a "snapshot" file. Then, all the simulation can start from the recorded settings and data. Control parameters are updated every 0.2 seconds. After each simulation, the obtained cost is compared to the previous best values. The authors used the *Multirun* function from the PSCAD library to rerun the simulation multiple times. The PSO algorithm is implemented in the ANSI C-code functions and integrated with PSCAD simulations.

IV. Case Studies

The microgrid system model shown in Fig. 1 has been implemented using PSCAD/EMTDC. The model contains two inverter-interfaced DGs with three-level PWM voltage source inverters. The DGs are coordinated via droop controllers and a supervisory centralized controller. Hence, the adjustments in voltages and system frequency are restored close to nominal values by the load reference signals sent by the supervisory controller.

As explained in section III, the microgrid DG controllers are optimized in two steps. First, the inverter output controller is optimized. The small-signal model of the inverter and the rest circuits described as (19) and (20) can be obtained from the operating condition data listed in Table I, which shows the microgrid system parameters of three different operating conditions such as a grid-connected case and two different loading cases of island modes. Then, the cost function of (30) is minimized considering individual inverter stability and robustness.

Fig. 8 shows the optimization procedure of the inverter output controller. Identical PI controllers are used as the *d*- and *q*-axis current controllers. The particles for PSO1 and PSO2 are defined as $[K_p, K_i]$ and $[\alpha]$. The population sizes and the total iteration number are set to 10 and 200 for PSO1 and 5 and 100 for PSO2, respectively. As a result, the optimal control parameters are $[K_p, K_i] = [15.11, 100.00]$.

The second process is to optimize the droop controller considering the power sharing performance and stable operation of the overall microgrid system by minimizing the cost function of (34). During this optimization process, the parameters of the individual inverter output controllers are set to the optimization result of inverter output controllers. Both grid-connected and island modes as well as transients during mode transition periods and abrupt load changes are considered in time-domain simulations. The obtained optimal droop control parameters are $[R_o, M_o] = [0.683, 15.582]$.

To gain good performance for different operating conditions, two solutions can be adopted. One solution is to change control gains (control parameters) dynamically and the other is to tune the gains so that the controller is robust for operating condition changes. Limited by control structure, the PI based controls' adaptability is limited. This paper adopts the second method, which is to find a good set of control parameters robustly tuned for different operating conditions.

Figs. 9 to 12 show the simulation verification of the microgrid operation with the optimal control parameters. The simulation sequence is as follows:

- *0.0 to 0.3 sec* (simulation initialization period): Load1 and Load2 are set to 2.0 MW and 1.0 MVar each (4.0 MW and 2.0 MVar in total). The outputs of the DGs are set to zero.
- *0.3 sec*: The power inverters of DG1 and DG2 start generating real and reactive power as much as 1.5 MW and 1.0 MVar each. (Grid-connected mode)
- *0.6 sec*: The inter-tie breaker disconnects the microgrid from the grid so that the microgrid switches to the island mode. (Island mode)
- *0.9 sec*: The load reference signals are sent to the droop controllers of DGs to restore nominal voltage and fre-

TABLE 1 MICROGRID PARAMETERS IN PER UNIT

	Grid-connected mode	*Island mode #1*	*Island mode #2*
P_{DG1}, Q_{DG1}	0.75, 0.50	1.00, 0.50	0.50, 0.25
P_{DG2}, Q_{DG2}	0.75, 0.50	1.00, 0.50	0.50, 0.25
P_{load1}, Q_{load1}	1.00, 0.50	1.00, 0.50	1.00, 0.50
P_{load2}, Q_{load2}	1.00, 0.50	1.00, 0.50	0.00, 0.00
P_{grid}, Q_{grid}	0.50, 0.00	0.00, 0.00	0.00, 0.00
R_{sys}	0.0046	0.0071	0.0071
L_{sys}	0.0100	0.0052	0.0052
R_{load}	0.6913	0.4009	0.8019
L_{load}	0.2788	0.2020	0.4040
R_{inv}	0.0033	0.0033	0.0033
L_{inv}	0.9008	0.9008	0.9008
I_{sys}^{d}, I_{sys}^{q}	0.50, 0.00	1.00, -0.50	0.50, -0.25
I_{load}^{d}, I_{load}^{q}	1.25, -0.50	2.00, -1.00	1.00, -0.50
I_{inv}^{d}, I_{inv}^{q}	0.75, -0.50	1.00, -0.50	0.50, -0.25

(All units are p.u. where P_{rated} = 2MW, V_{rated} = 13.8kV and F_{rated} = 60Hz.)

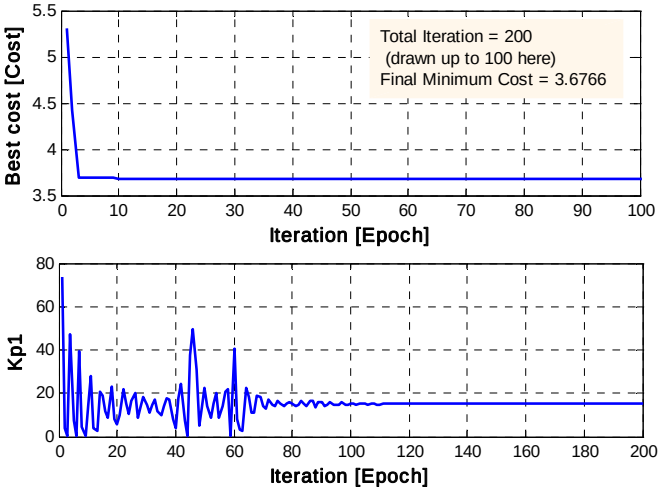

Fig. 8 PSO optimization process: (a) Global-best fitness search process (upper), (b) Search process of Kp1 of a particle (bottom)

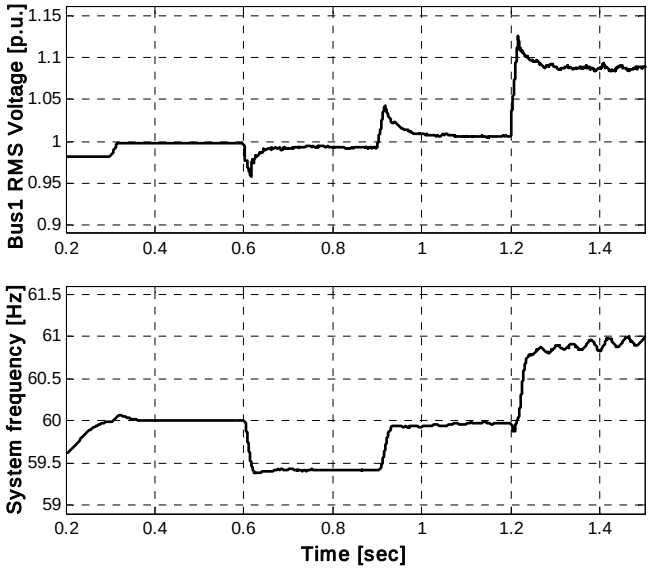

Fig. 9 RMS Bus1 voltage and system frequency

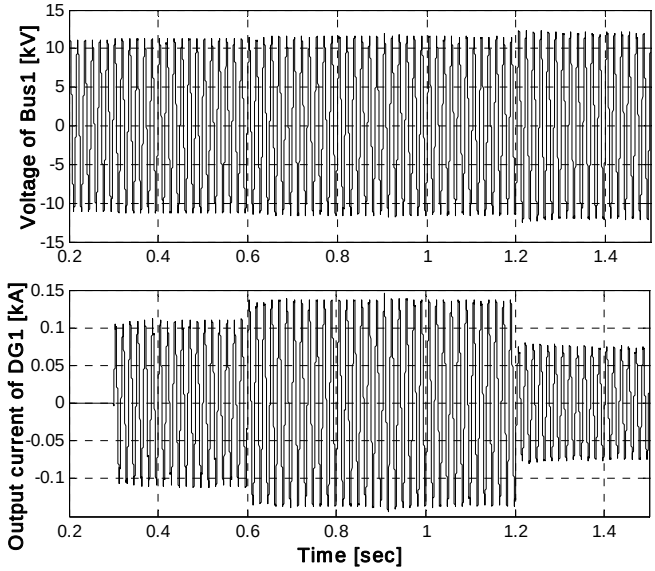

Fig. 11 Bus1 voltage waveform and inverter output current waveform

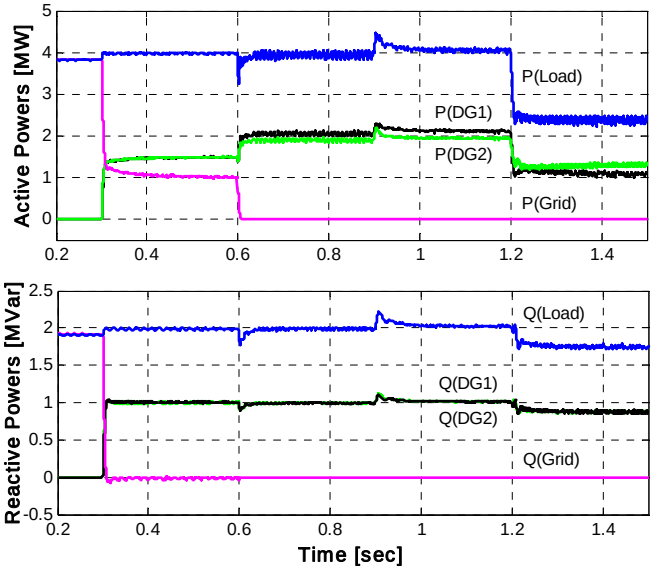

Fig. 10 Active and reactive power measurement: power consumed by loads, power generated by DGs, and power supplied from the grid side

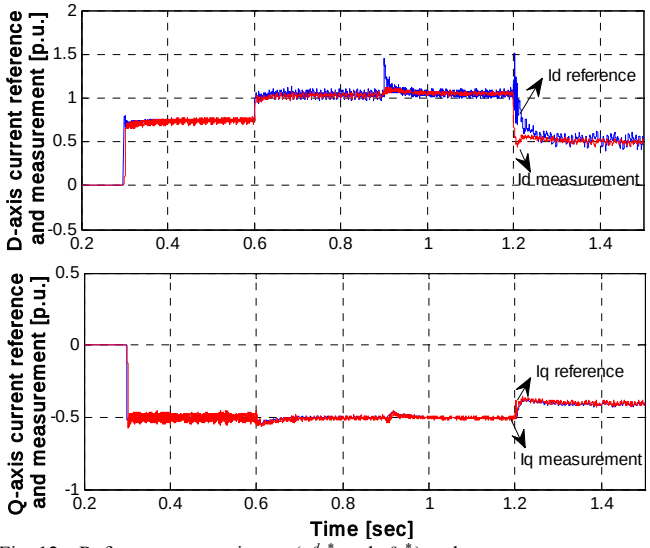

Fig. 12 Reference current inputs ($i_{inv}^{d\ *}$ and $i_{inv}^{q\ *}$) and measurements (i_{inv}^{d} and i_{inv}^{q}) of inverter current controller

quency values.

- *1.2 sec*: The local loads suddenly decrease. (Load variation in island mode)

Fig. 9 shows the bus rms voltage and system frequency variation during the simulation. In the grid-connected mode, the bus voltage and system frequency are well maintained around the nominal values (1.0 p.u. and 60 Hz). However, in the island mode, they vary according to the instant power mismatch and the droop control characteristics. At 0.9 seconds, the voltage and frequency are restored close to the nominal values by the load reference signals.

Fig. 10 shows the simulation results of real and reactive power. Note that both real and reactive power control performance are stable due to optimization using an error-integrating type cost function. Fig. 11 shows the voltage and current waveforms.

Fig. 12 shows the control performance of the inverter current controller. The q-axis current signals are negative due to the signal convention of the d-q transformation used in this paper as explained in the Appendix. The d-q current reference signals are from the droop controllers. Since the bus voltage is around 1.0 p.u., the per-unit values of the d- and q-axis currents are similar to real and reactive power, respectively.

V. Conclusions

In this paper, microgrid DG controllers are designed and optimized. Coordination between multiple DGs in a microgrid system can be realized by using droop controllers, which can automatically find the amount of power sharing so that the

microgrid can be stabilized quickly. The droop constants are optimized by Particle Swarm Optimization with power-electronic-switch-level simulations.

For the inverter output controllers, robust controller design scheme has been proposed. To deal with persistent voltage and frequency disturbances in a microgrid, L_1 robust control theory with the double-layer PSO algorithm has been proposed. The double-layer PSO algorithm finds the tightest bound of the L_1 system operator norm so that the closed-loop system is robust to exogenous disturbances such as bus voltage and frequency variations. The system nonlinearity is accommodated by considering various power system operating conditions.

VI. Appendix

• *D-q transformation*

The transformation from a-b-c reference frame to d-q rotating reference frame can be obtained as

$$X^{dq} = C_1 \cdot X^{abc} \tag{A1}$$

where $C_1 = \frac{2}{3}\cdot\begin{bmatrix} cos(\theta) & cos(\theta-\frac{2\pi}{3}) & cos(\theta+\frac{2\pi}{3}) \\ -sin(\theta) & -sin(\theta-\frac{2\pi}{3}) & -sin(\theta+\frac{2\pi}{3}) \end{bmatrix}$.

Then, the d-axis phasor in the d-q reference frame is aligned to the rotating phase-a phasor of the a-b-c reference frame and the q-axis phasor leads π/2 from the d-axis phasor. If the d-axis is aligned to the phase-a voltage phasor, then the d-axis current accounts for the real power and the q-axis current is the reactive current as

$$P \approx \frac{3}{2} v_d i_d,\ Q \approx -\frac{3}{2} v_d i_q \tag{A2}$$

where the sign convention of reactive power is positive for inductive reactive power.

• *Sensitivity of control modes to control parameters*

The sensitivity of the control mode whose eigenvalue is λ_i to the control parameter c_k can be defined as

$$p_{ki} = \frac{\partial \lambda_i}{\partial c_k} \tag{A3}$$

• *Vector norms*

Two ∞-norms of continuous-time vector $y(t),\ w(t) \in R^n$ are defined as

$$\|y\|_{\infty,\infty} = \sup_{-\infty<t<\infty} \|y(t)\|_\infty \tag{A4}$$

$$\|w\|_{\infty,2} = \sup_{-\infty<t<\infty} \|w(t)\|_2 \tag{A5}$$

The finite norm value means that the vector variables are bounded. Then, we can also write $y \in L_{\infty,\infty}$ and $w \in L_{\infty,2}$, respectively. Although the two definitions of ∞-norms look different, they define the same kind of sets. The reason of using two different forms of norms is for mathematical convenience to derive the maximum bound [15].

• *Proof of equation (21), the bound for the L_1 norm*

From (19) and (20), the performance variable vector can be presented as

$$y(t) = (G * w)(t) + D_{cl} \cdot w(t) \tag{A6}$$

where, $G(t) = C_{cl} e^{A_{cl} t} B_{cl}$ and $w(t) \in L_{\infty,2}$. Then, the norm of the performance variable vector can be bounded as

$$\|y\|_{\infty,\infty} \le \|G * w\|_{\infty,\infty} + \|D_{cl} \cdot w\|_{\infty,\infty} \tag{A7}$$

According to [15], the elements of the right-hand side of (A7) are bounded as

$$\|G * w\|_{\infty,\infty} \le \sigma_{max}^{1/2}\left(C_{cl} Q C_{cl}^T\right)\|w\|_{\infty,2} \tag{A8}$$

$$\begin{aligned} \|D_{cl} \cdot w\|_{\infty,\infty} &= \sup_{-\infty<t<\infty} \|D_{cl} \cdot w(t)\|_\infty \le \sup_{-\infty<t<\infty} \|D_{cl}\|_{\infty,2} \cdot \|w(t)\|_2 \\ &= \|D_{cl}\|_{\infty,2} \|w\|_{\infty,2} = \sigma_{max}^{1/2}\left(D_{cl} D_{cl}^T\right)\|w\|_{\infty,2} \end{aligned} \tag{A9}$$

Therefore, by applying (A7) and (A8) to (A6), we can get

$$\|G\|_1 \le \sigma_{max}^{1/2}\left(C_{cl} Q C_{cl}^T\right) + \sigma_{max}^{1/2}\left(D_{cl} D_{cl}^T\right) \tag{A10}$$

VII. References

[1] R.H. Lasseter, "Control and Design of Microgrid Components," PSERC Final Report, Jan. 2007.

[2] N. Hatziargyriou, H. Asano, R. Iravani, and C. Marnay, "Microgrids," IEEE power & energy magazine, pp.78-94, Jul./Aug. 2007.

[3] F. Katiraei, M.R. Iravani, "Power management strategies for a Microgrid with multiple distributed generation units," IEEE Trans. Power Systems, vol. 21, no. 4, pp.1821-1831, Nov. 2006.

[4] N. Pogaku, M. Prodanovic, and T. Green, "Modeling, analysis and testing of autonomous operation of an inverter-based microgrid," IEEE Trans. Power Electronics, vol. 22, no. 2, pp. 613-625, Mar. 2007.

[5] F. Katiraei, and M.R. Iravani, "Micro-Grid autonomous operation during and subsequent to islanding process," *IEEE Trans. Power Delivery*, vol. 20, no. 1, Jan. 2005, pp.248-257.

[6] I. Chung, S. Park, H. Kim, S. Moon, B. Han, J. Kim, and J. Choi, "Operating strategy and control scheme of premium power supply interconnected with electric power systems," *IEEE Trans. Power Delivery*, vol. 20, no. 3, pp. 2281-2288, Jul. 2005.

[7] M. Chandorkar, D. Divan, and B. Banerjee, "Control of distributed UPS systems," *IEEE PESC'94*, 1994, pp. 197-204.

[8] J. Guerrero, L. Na, M. Castilla, and J. Miret, "A wireless controller to enhance dynamic performance of parallel inverters in distributed generation systems," *IEEE Trans. Power Electronics*, vol. 19, no. 5, Sep. 2004, pp. 1205-1213.

[9] K. De Brabandere, B. Bolsens, J. Van den Keybus, A. Woyte, J. Driesen, R. Belmans, "A Voltage and Frequency Droop Control Method for Parallel Inverters" *IEEE Trans. Power Electronics*, vol. 22, no. 4, pp. 1107-1115, Jul. 2007.

[10] P. Kundur, Power System Stability and Control, McGraw Hill, 1994.

[11] J.B. Burl, Linear Optimal Control – H_2 and H_∞ Methods, Addison-Wesley, 1999.

[12] Y.W. Li, D.M. Vilathgamuwa, and P.C. Loh, "Robust Control Scheme for a Microgrid With PFC Capacitor Connected," IEEE Trans. Industry Applications, vol. 43, no. 5, pp. 1172-1182, Sep./Oct. 2007.

[13] M. Vidyasagar, "Optimal Rejection of Persistent Bounded Disturbances," IEEE Trans. Automatic Control, vol. AC-31, no. 6, pp. 527-534, Jun. 1986.

[14] W.M. Haddad, and V. Chellaboina, "Mixed-Norm H2/L1 Controller Synthesis via Fixed-Order Dynamic Compensation: A Riccati Equation Approach," Proceedings of the 36th Conference on Decision & Control, pp. 452-457, Dec. 1997.

[15] V.S. Chellaboina, W.M. Haddad, and J.H. Oh, "Fixed-order dynamic compensation for linear systems with actuator amplitude and rate saturation constraints," International Journal of Control, vol. 71, no. 12, pp/1087-1103, 2000.

[16] T.D. Curry, and E.G. Collins, Jr., "Robust l_1 design of a multivariable PI controller using a real-coded genetic algorithm," Proceedings of the 2005 American Control Conference, vol. 6, pp. 4295-4300, 8-10 Jun. 2005.

[17] I. Chung, W. Liu, D.A. Cartes, and K. Schoder, "Control Parameter Optimization for a Microgrid System Using Particle Swarm Optimiza-

tion," IEEE International Conference on Sustainable Energy Technologies (ICSET 2008), Singapore, Nov. 2008.
[18] E. Barklund, N. Pogaku, M. Prodanovic, C. Hernandex-Aramburo, and T.C. Green, "Energy Management in Autonomous Microgrid Using Stability Constrained Droop Control of Inverters," IEEE Trans. on Power Electronics, vol. 23, no. 5, pp. 2346-2352, Sep. 2008.
[19] I. Chung and S. Moon, "A new islanding detection method using phase-locked loop for inverter-interfaced distributed generators," *Journal of Electrical Engineering & Technology*, vol. 2, no. 2, pp.165-171, Jun. 2007.
[20] C. Schauder and H. Mehta, "Vector analysis and control of advanced static VAR compensators," *IEE Proceedings-C*, vol. 140, No. 4, July, 1993, pp. 299-306.
[21] J. Kennedy and R. C. Eberhart, "Particle swarm optimization," in Proc. of International Conference on Neural Network (ICNN), vol. 4, pp. 1942-1948, Perth, Australia, 1995.
[22] J. Robinson and Y. Rahmat-Samii, "Particle swarm optimization in electromagnetics," IEEE Trans. Antennas and Propagation, vol.52, no.2, pp.397-407, Feb. 2004.
[23] I. Chung, W. Liu, S. Leng, M. Andrus, D.A. Cartes, M. Steurer and K. Schoder, "Integration of a bi-directional DC-DC converter model into a large-scale system simulation of a shipboard MVDC power system," IEEE Electric Ship Technologies Symposium (ESTS 2009), Apr. 20-22, 2009.
[24] N. Killingsworth and M. Krstic, "Auto-tuning of PID controllers via extremum seeking," *American Control Conference* 2005, pp. 2251-2256.

VIII. BIOGRAPHIES

Il-Yop Chung (S'01-M'08) received his B.S., M.S., and Ph.D. degrees in electrical engineering from Seoul National University, Seoul, Korea, in 1999, 2001, and 2005, respectively. He was a Postdoctoral Associate at Virginia Tech, Blacksburg, VA, from 2005 to 2007. He was also a Visiting Researcher at ABB US Corporate Research Center, Raleigh, NC in 2007. Currently, he is an Assistant Scholar Scientist with the Center for Advanced Power Systems (CAPS) at Florida State University, Tallahassee, FL. His research interests are power quality, distributed energy resources, renewable energy, and shipboard power systems.

Wenxin Liu (S'01-M'05) received his Ph.D. degree in Electrical Engineering from Missouri University of Science and Technology (formerly University of Missouri-Rolla), Rolla, MO in 2005. He received his B.S. and M.S. degrees from Northeastern University, China in 1996 and 2000, respectively. From 2005 to 2009, he was an Assistant Scholar Scientist with the Center for Advanced Power Systems (CAPS) at Florida State University, Tallahassee, FL. He is currently an Assistant Professor of the Klipsch School of Electrical and Computer Engineering at New Mexico State University, Las Cruces, NM. His current research interests include neural network control, swarm intelligence, control and optimization of microgrid, and renewable energy.

David A. Cartes (S'97-A'99-M'03-SM'07) received the Ph.D. degree in engineering science from Dartmouth College, Hanover, NH. He is an Associate Professor of the Department of the Mechanical Engineering at Florida State University (FSU), Tallahassee, FL from January 2001. He heads the Power Controls Lab at the Center for Advanced Power Systems. He is also the director of the Institute for Energy Systems, Economics and Sustainability (IESES) at FSU. His research interests include distributed control and reconfigurable systems, real-time system identification, and adaptive control. In 1994, he completed a 20-year U.S. Navy career with experience in operation, conversion, overhaul, and repair of complex marine propulsion systems. He is a member of the American Society of Naval Engineers.

Emmanuel G. Collins, Jr. (S'83–M'86–SM'99) received the B.S. degree from Morehouse College, Atlanta, GA, in 1981, the B.M.E. degree from the Georgia Institute of Technology, Atlanta, in 1981, the M.S. degree in mechanical engineering from Purdue University, West Lafayette, IN, in 1982, and the Ph.D. degree in aeronautics and astronautics from Purdue University in 1987. He worked for seven years in the Controls Technology Group at Harris Corporation, Melbourne, FL before joining the Department of Mechanical Engineering at the Florida A&M University – Florida State University College of Engineering, Tallahassee, FL, where he currently serves as John H. Seely Professor and Director of the Center for Intelligent Systems, Control and Robotics (CISCOR). His current research interests include navigation and control of autonomous vehicles (ground, water and air) in extreme environments and situations, multi-robot and human-robot cooperation, control of aero-propulsion systems, and applications of robust control. He is the author of over 200 technical publications in control and robotics and served as an associate editor of the IEEE Transactions on Control System Technology from 1992 to 2001. In 1991 he received the Honorary Superior Accomplishment Award from NASA Langley Research Center for "contributions in demonstrating active control of flexible spacecraft."

Seung-Il Moon (M'93) received the B.S. degree in electrical engineering from Seoul National University, Seoul, Korea, in 1985, and the M.S. and Ph.D. degrees in electrical engineering from Ohio State University, Columbus, OH, in 1989 and 1993, respectively. Currently, he is a Professor of the School of Electrical Engineering and Computer Science at Seoul National University. He is the Editor-in-Chief of Journal of Electrical Engineering and Technology and also the Vice Chairman of Editorial Board of the Korean Institute of Electrical Engineers (KIEE) since 2008. His special fields of interest include power quality, flexible ac transmission system, renewable energy, and distributed generation.